Supplementary Information

Dual-Function Electrochemical Cell for Simultaneous Carbon Capture and Lithium Extraction from Saline Waters

Omer Shinnawy, Seyyed Arman Hejazi, Kiana Amini*

Department of Materials Engineering, The University of British Columbia, 6350 Stores Road, Vancouver, BC V6T 1Z4, Canada

* *Corresponding author. E-mail address: kiana.amini@ubc.ca*

1. Thermodynamic Analysis

This section outlines the details, assumptions, and parameters used in the dual-function electrochemical thermodynamic model.

1.1 Dissolved inorganic carbon composition in simulated seawater

An open-system simulated seawater consisting of 0.5M NaCl and seawater pH ~8.06 is used to solve for the unknown concentration of the dissolved inorganic carbon (DIC) using equations S1-S5:

$$[H^+] + [Na^+] = [Cl^-] + [HCO_3^-] + 2[CO_3^{2-}] + [OH^-] \quad \text{(S1)}$$

$$C_{DIC} = [CO_2] + [HCO_3^-] + [CO_3^{-2}] \quad \text{(S2)}$$

$$[CO_2(aq)] = P_{CO2} * C_{Henry} \quad \text{(S3)}$$

$$[HCO_3^-] = \frac{Ka_1 * P_{CO_2} * C_{Henry} * \gamma_{CO_2}}{\gamma_{HCO_3^-} * \gamma_{H^+}} * \frac{1}{[H^+]} \quad \text{(S4)}$$

$$[CO_3^{2-}] = \frac{Ka_1 * Ka_2 * P_{CO2} * C_{Henry} * \gamma_{CO2}}{\gamma_{CO_3^{2-}} * \gamma_{H^+}^2} * \frac{1}{[H^+]^2} \quad \text{(S5)}$$

Henry's constant (C_{Henry}) and water dissociation constant (K_W) are taken at 0.033 M/bar and 10^{-14} M^2 respectively. The temperature (T) is set at 298.15 K, and the CO_2 partial pressure in an open system is set at 0.42 mbar. Dickson & Millero's formulation is used to calculate the H_2CO_3 acid dissociation constant (K_{a1}^*) and HCO_3^- acid dissociation constant (K_{a2}^*) as a function of salinity (S) in practical salinity unit (PSU) , accounting for it's effect on activity coefficients, are:

$$K_{a1}^* = 10^{-(\frac{845}{T} + 3.284 - 0.0098S + 8.7x10^{-5}S^2)} \quad \text{(S6)}$$

$$K_{a2}^* = 10^{-(\frac{1377.3}{T} + 4.824 - 0.01855S + 1.22x10^{-4}S^2)} \quad \text{(S7)}$$

Salinity is calculated from the ionic strength (I) in mol/L with the direct conversion to mol/kg assuming solution density ≈ water density of 1 kg/L, and Na^+ and Cl^- are the dominant contributors [1]:

$$S = \frac{1000I}{19.924 + 1.005I} \quad \text{(S8)}$$

$$I = \frac{1}{2}\sum c_i Z_i^2 \quad \text{(S9)}$$

Solving all the unknowns gives the following outcome: $[Na^+]$ = 502.243 mM, [DIC] = 2.069 mM, $[CO_3^{2-}]$ = 0.186 mM and $[HCO_3^-]$ = 1.869 mM, with a charge balance error of $-1.0* 10^{-16}$ M. These values are within 1% of the DIC and it's speciation concentrations found naturally in seawater, validating the usage of the Dickson & Millero formulation for analyzing DIC speciation. Using this model, a Bjerrum plot showing DIC composition at equilibrium as a function of pH is plotted.

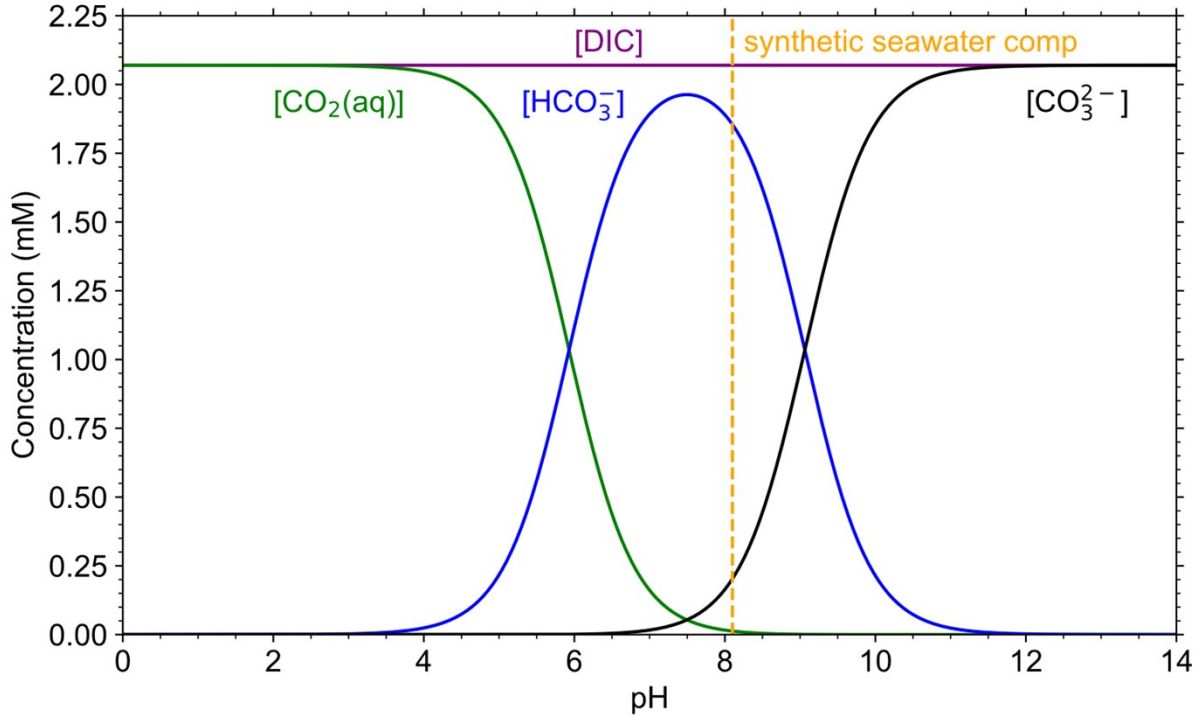

Fig. S1: Thermodynamic modelling of dissolved inorganic carbon as a function of pH.

1.2 Millero and Schreiber method to estimate activity coefficients for lithium, chloride, and protons based on salinity

For the acidification and alkalization steps thermodynamic analysis, the bismuth chamber is supplied with an electrolyte containing 500 mM Cl^- and 502.243 mM Na^+, with a DIC of 2.069 mM initially that is acidified and then alkalinized after CO_2 has been captured. For the extraction step ,lithium side initially contains 500 mM Cl^- and 500 mM Na^+ and a lithium concentration of

0.17 ppm or 50 ppm. The recovery step is done in a solution that contains varying concentration of lithium chloride, starting with a basis of 10^{-10} M. The activity coefficients, γ_i, are computed from the extended Debye-Hückel expression with empirical corrections:

$$\ln \gamma_i = Z_i^2 f_\gamma + IB_0 + f_1 B_1 + I^2 C \tag{S10}$$

where c_i is the concentration of species i and Z_i is the charge of species i. Additionally:

$$f_\gamma = -A_{DH}\left(\frac{\sqrt{I}}{1+1.2\sqrt{I}} + \frac{2}{1.2}\ln\left(1+1.2\sqrt{I}\right)\right) \tag{S11}$$

$$f_1 = 1 - \exp\left(-2\sqrt{I}\right).\left(1+2\sqrt{I}-2I\right) \tag{S12}$$

where A_{DH}=0.392 is the Debye-Hückel constant at 25°C. The rest of the constants are provided in the table below.

Table S1:Debye-Hückel constants for ions in the system

Species	Z	B_0	B_1	C
H^+	+1	0.6133	0.1884	0.00366
Cl^-	−1	0.0967	0.1061	−0.00126
Li^+	+1	0.5009	0.2013	0.01203

1.3 Derivation of the quartic equation for [H^+]

To determine the distribution of DIC species and pH, we solve for the hydrogen ion concentration [H^+] using charge and mass balance relationships, along with the known equilibrium constants (equations S1-S5). Each species is related to [H^+] and the partial pressure of CO_2 (P_{CO_2}) through equilibrium and are substituted into the DIC expression and rearranged to solve for [H^+] implicitly. After rearranging and combining with charge neutrality constraints, we arrive at a quartic polynomial equation in [H^+]:

$$A[H^+]^4 + B[H^+]^3 + C[H^+]^2 + D[H^+] + E = 0 \tag{S13}$$

$$A = C_{Henry} \tag{S14}$$

$$B = C_{Henry} * [Na^+]_{neg} - C_{Henry} * [Cl^-]_{neg} + K_{a1}^* * C_{Henry} \tag{S15}$$

$$C = -C_{Henry} * K_w + K_{a1}^* * C_{Henry} * ([Na^+]_{neg} - [Cl^-]_{neg} + K_{a2}^* - [DIC]_0) \tag{S16}$$

$$D = -K_{a1}^* * C_{Henry} * K_w + K_{a2}^* * K_{a1}^* * C_{Henry} * ([Na^+]_{neg} - [Cl^-]_{neg} - 2[DIC]_0) \tag{S17}$$

$$E = -K_{a2}^* * K_{a1}^* * C_{Henry} * K_w \tag{S18}$$

This polynomial is solved numerically (e.g., using NumPy's np.roots function) at each simulation step to find the physically meaningful, positive real root corresponding to the $[H^+]$, which is then used to compute all the unknown concentrations, and determine the work requirements as the operating conditions or initial conditions are varied.

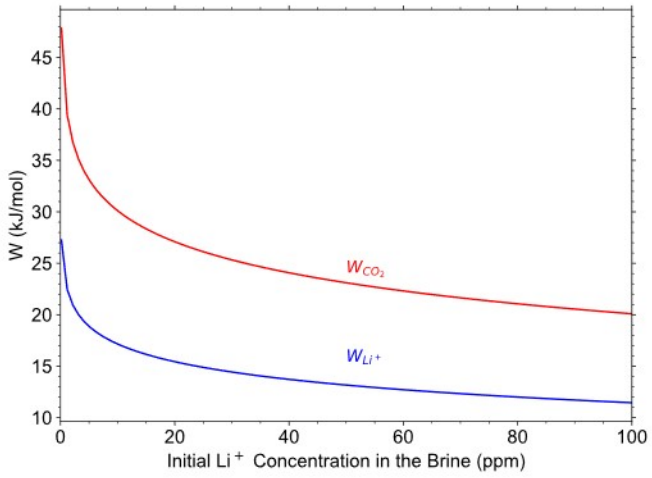

Fig. S2: Calculated thermodynamic work per mole of CO_2 and Li^+ as a function of initial lithium concentration in the source water.

a)

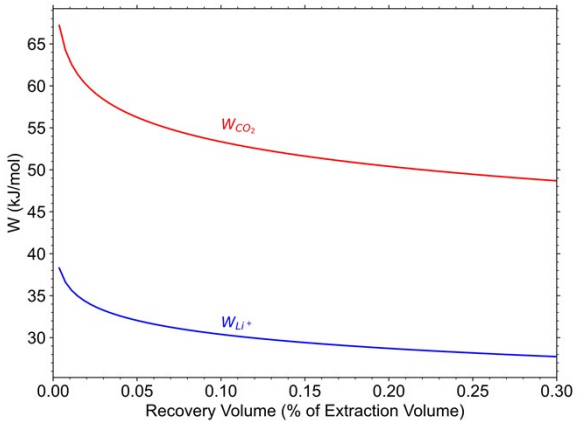

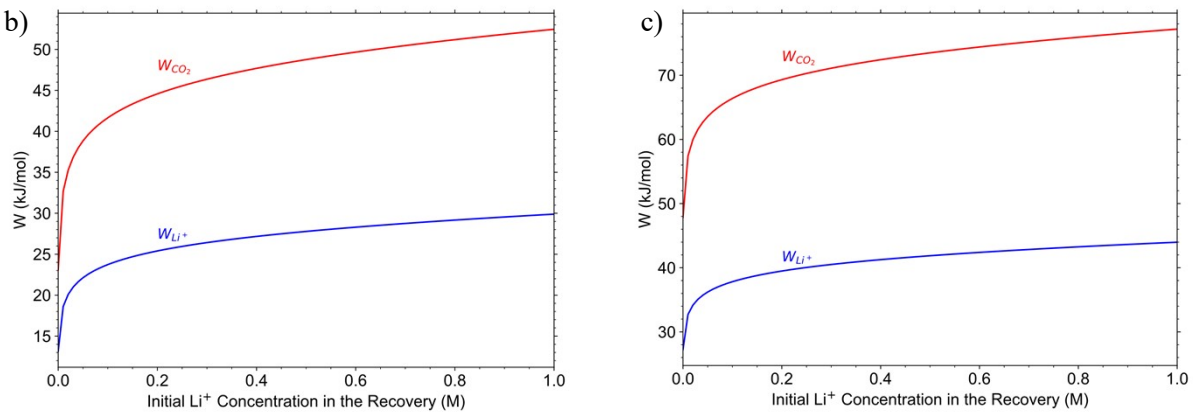

Fig. S3: a) Calculated thermodynamic work per mole of CO_2 and Li^+ as a function of recovery volume used as a percentage of the extraction volume on the lithium side. b) Calculated thermodynamic work per mole of CO_2 and Li^+.

2. Half-cell Study

2.1 Electrode preparation

Electrodes were prepared by creating a slurry composed of active material (LFP or Bi), conductive material (carbon black) and binder (PVDF) at a ratio of 8:1:1 mixed with the solvent, N-Methylpyrrolidone (NMP), using a mortar and pestle. For LFP and Bi slurry, the solid-to-liquid ratio is 1.75 µl/mg and 1.50 µl/mg respectively. The electrode substrate used is 2x2 cm^2 Fuel Cell Store carbon paper, Sigracet 28AA coated with the slurry layer-by-layer using tape and a spatula. Coated electrodes are dried overnight at 80°C to evaporate NMP. LFP electrodes are dried at −1atmg, while bismuth electrodes at atmospheric pressure. The active mass loading after preparation is 25 mg/cm^2 for LFP and 12 mg/cm^2 for bismuth

2.2 Pretreatment & cyclic voltammograms

For pretreatment, LFP is delithiated to 50% of its capacity based on it's mass loading. This frees up intercalation sites for lithium to intercalate into, while having lithium in the iron phosphate structure as seeds, hindering the intercalation of other cations into the structure [2]. The potentiostat used for all experiments is a 2-channel Biologic SP-300 Potentiostat set to operate in floating mode. The delithiation occurs in an H-cell of 50 ml 0.5M NaCl in each chamber separated by an anion exchange membrane, Selemion DSVN. The working electrode is the prepared LFP, the counter electrode is a carbon rod, and the reference electrode is Ag/AgCl in 1M KCl. The pretreatment process is operated as chronoamperometry at 1V vs. Ag/AgCl, until 50% of the charge calculated from active material loading has passed. Cyclic voltammogram of a pre-treated LFP is operated in a similar set-up with the settings of 0.2 mV/s from +1.0 V to −1.0 V vs. Ag/AgCl. For bismuth, the pretreatment procedure is a 3-cycle cyclic voltammogram in a similar H-cell set-up operated at 2 mV/s from −1.9 V to +1.0 V vs. Ag/AgCl. This activates the bismuth electrode and lowers the overpotentials when operated.

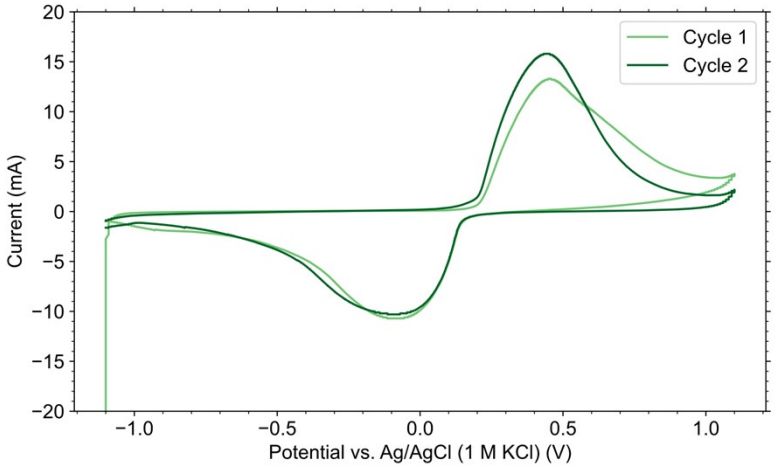

Fig. S4: Cyclic voltammograms of the prepared unpretreated LFP electrode in 0.5 M LiCl at a scan rate of 0.2 mV/s from −1.1V to +1.1V vs vs. Ag/AgCl, showing lithium intercalation/deintercalation peaks over two consecutive cycles in the absence of sodium with an average charge ratio passed during oxidation and reduction of 1.01.

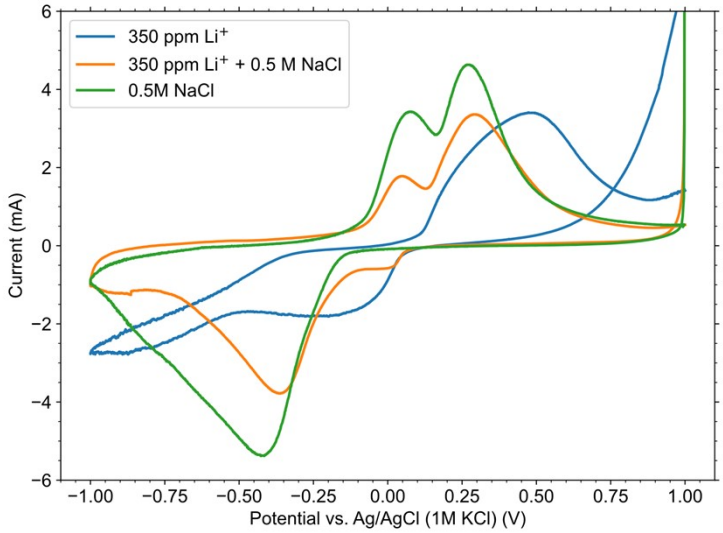

Fig. S5: Cyclic voltammograms 1st cycle of the prepared unpretreated LFP electrodes in 350 ppm Li^+, 350 ppm Li^+ + 0.5 M NaCl, and 0.5 M NaCl electrolytes at a scan rate of 0.2 mV/s, showing differences in redox behavior under varying ionic compositions.

3. H-Cell Study

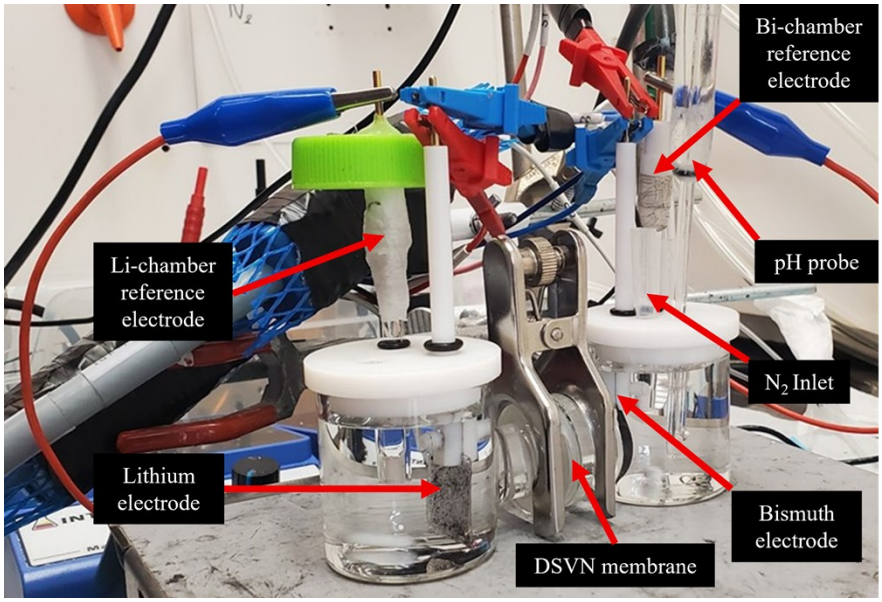

Fig. S6: H-cell setup for testing lithium and bismuth electrode operation

Fig. S6 shows the set-up used for the pairing of the LFP and Bi electrodes in an H-cell. A 1M Ag/AgCl is used to measure the half-cell voltage in each chamber. The cell operation is controlled by varying the current direction from the lithium chamber using a channel potentiostat cable, while the other channel is used to measure the half-cell voltage of the bismuth electrode. During the runs, an Arduino board with a data logger, CoolTerm, is used to operate additional equipment and store the data. In the bismuth chamber, pH measurement is achieved using a Mettler Toledo LE422, and N_2 is purged at 30 sccm using a Sierra mass flow controller. Magnetic stirrer bars at 700 rpm ensure a homogeneous solution for operation. For the DIC-free test, 0.5M NaCl was used in bismuth chamber and 0.5M LiCl was used in the lithium chamber. Operation was shifted between extraction/acidification or recovery/alkalization based on the pH in the bismuth chamber, and without replacing the chambers' electrolytes. For the test shown in Fig 3, 350 ppm lithium and 0.5M NaCl for the lithium chamber, and 0.25mM DIC (0.22mM $NaHCO_3$ and 0.03Mm Na_2CO_3) and 0.5M NaCl for the bismuth chamber were used. Samples taken from lithium chamber are diluted using 2% nitric acid to the ppb range of Thermo Scientific iCAP Qc Inductively Coupled Plasma Mass Spectrometer (ICP-MS) to determine the change in lithium concentration.

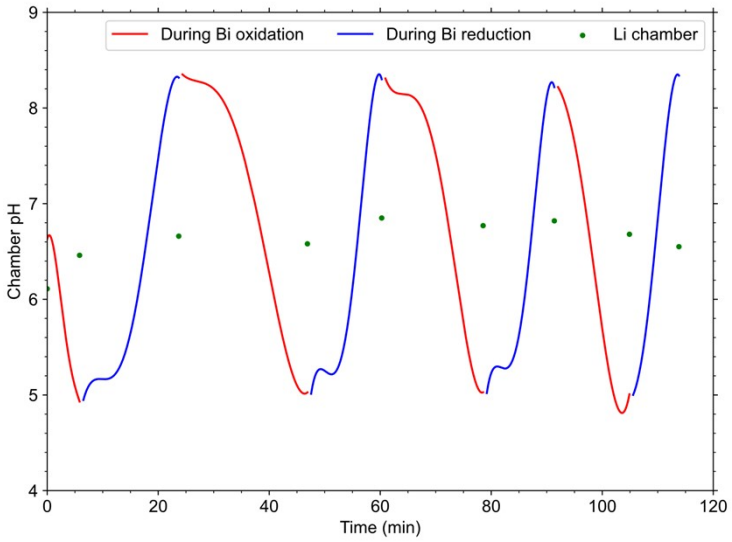

Fig. S7: Real-time pH monitoring of the bismuth side during consecutive Bi oxidation (acidification) and reduction (alkalization) cycles, with pH in the lithium chamber measured before and after each step.

4. Flow-Cell Study

4.1 Experimental setup

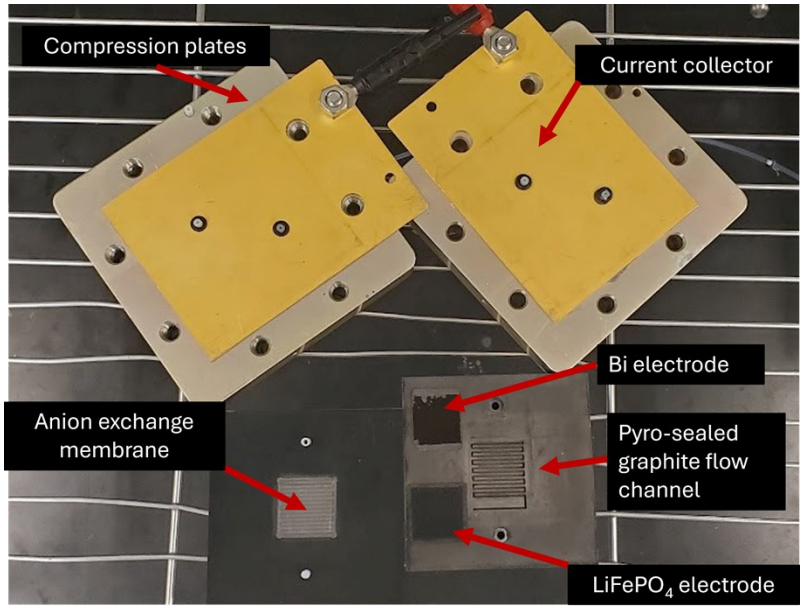

Fig. S8: Components of a zero-gap flow cell

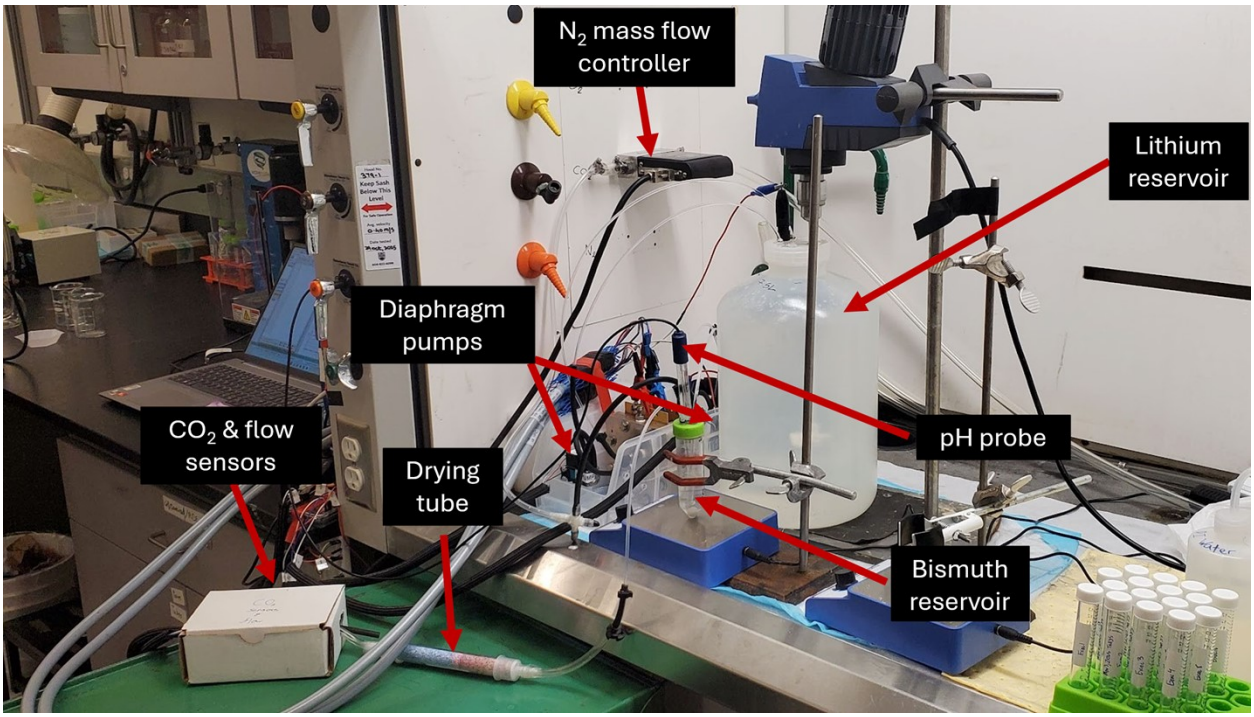

Fig. S9: Testing station for the dual-function flow cell.

The flow cell used is zero-gap flow cell with a pyro-sealed graphite serpentine flow channel. 4 cm^2 coated electrodes are used for testing, with the membrane-electrode assembly held in place by the compression plates tightened to 60 in-lb (Fig. S8). An Arduino board with a pH probe and N_2 are used on the bismuth reservoir, while adding an outlet gas line connected to a drying tube at the upstream of flow sensor, to ensure gas flow throughout the line, and an ExplorIR-M5% CO_2 sensor from CO2METER to record changes in the CO_2 molar composition during operation (Fig. S9). To draw the liquid from the reservoir to the flow cell and back to the reservoir, while maintaining an ionic conductive pathway between the reservoir and the flow cell, FF 12 DCB-4' diaphragm pumps from KNF are used. All electrical components were connected to the Arduino board for operation, while data logging occurs using the CoolTerm software. For operation, a potentiostat channel was used to apply current between the LFP and Bi electrode while measuring the voltage between the two electrodes, and another channel was used as a sense channel to measure voltage between an electrode and the reference electrode. Taking the difference between the voltage readings would give you the cell voltage, and two half-cell voltages. During operation, the first flow cell cycle where LFP and Bi are paired together is considered pretreatment.

Table S2: Comparison of natural seawater and simulated seawater

Concentration (mM)	**Li^+**	**Na^+**	**K^+**	**Mg^{2+}**	**Ca^{2+}**	**Cl^-**	**F^-**	**SO_4^{2-}**	**HCO_3^-**	**CO_3^{2-}**	**CO_2**
Natural Seawater[3]	0.024	481	10.5	54.1	10.5	559	0.07	28.9	1.89	0.189	0.013
Simulated Seawater	0.024	502	10.0	54.0	10.0	638	-	-	1.91	0.19	-

Table S3: Operation conditions during the extraction phase

Figure	**4**		**5**		**6a**		**6c**	
	Lithium	**Bismuth**	**Lithium**	**Bismuth**	**Lithium**	**Bismuth**	**Lithium**	**Bismuth**
Ions of interest	50 ppm Li^+	2.1 mM DIC	50 ppm Li^+	2.1 mM DIC	5 then 0.17 ppm Li^+	2.1 mM DIC	0.17 ppm Li^+	2.1 mM DIC
Other ions	Na^+ Cl^-	Na^+ Cl^-	Na^+ K^+ Mg^{2+} Ca^{2+} Cl^- DIC	Na^+ Li^+ K^+ Mg^{2+} Ca^{2+} Cl^-	Na^+ K^+ Mg^{2+} Ca^{2+} Cl^- DIC	Na^+ Li^+ K^+ Mg^{2+} Ca^{2+} Cl^-	Na^+ Cl^-	Na^+ Cl^-
Impurities addition	None		From the beginning		Last 2 cycles		None	
Reservoir volume	25 ml	25 ml	25 ml	25 ml	250ml, then 7.5 L	25 ml	7.5 L	25 ml
Flowrate (ml/min)	35	35	35	35	60	35	60	35

Before and after each recovery, ICP-MS samples are taken to calculate the change in the lithium concentration and pH probe is used to measure the pH in the lithium reservoir. In addition to convection mixing from the diaphragm pump, magnetic stirrer bars are used to ensure homogenous mixing. In the experiments with 7.5L of simulated seawater, impellers were used for mixing instead of stirrer bars. Table S2 shows the natural seawater composition and the simulated seawater tested. Table S3 summarizes the operating conditions during different extraction sets. For each recovery cycle set, 20 ml of 0.05M KCl with initially 0.17 ppm Li^+ is used (and re-used) for the lithium chamber, circulating at 35 ml/min. For bismuth chamber alkalization phase, 100 ml of pristine simulated seawater is used. If seawater impurities (K^+, Mg^{2+}, Ca^{2+}) are not present, the pristine seawater is mixed with the acidified seawater and circulated at 45 mL/min (Fig. S10). If impurities are present, acidified seawater is set aside for later use and the pristine seawater is circulated at 60 mL/min.

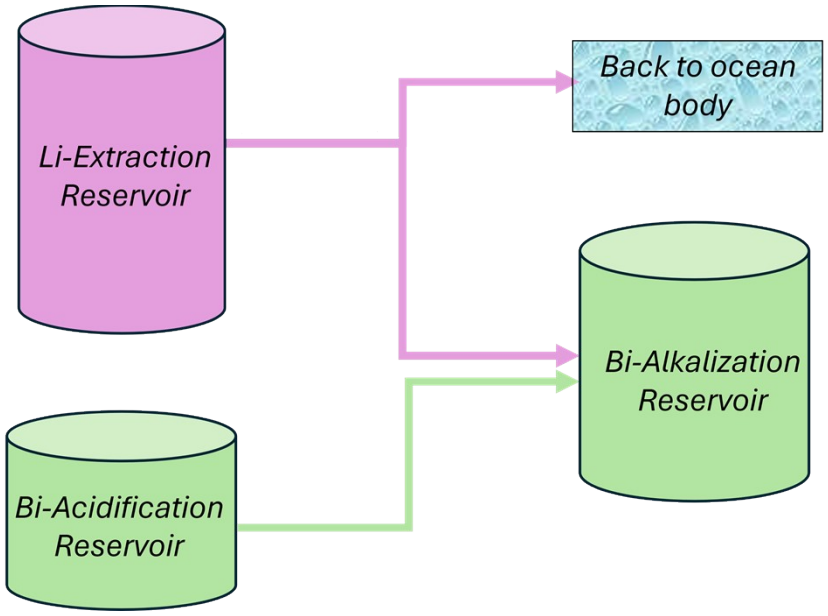

Fig. S10: Preparation of bismuth alkalization reservoir in the absence of impurities

4.2 Figure 4 additional data

For this test, the voltage is measured between the LFP and the 1M Ag/AgCl that was placed in the lithium reservoir during operation. The sense channel measured the voltage between LFP and Bi electrodes. The pH measured before and after each cycle is shown in Fig. S11 and S12.

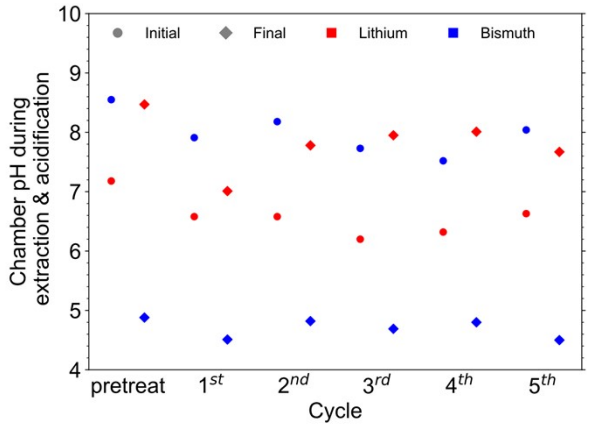

Fig. S11: Lithium and bismuth chamber pH in each cycle before and after extraction and acidification.

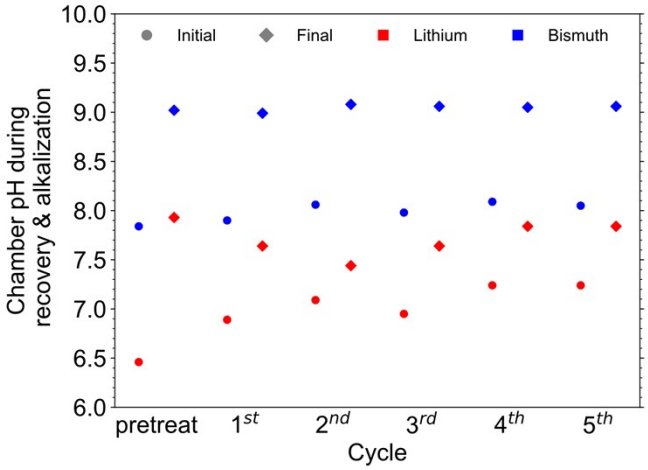

Fig. S12: Lithium and bismuth chamber pH in each cycle before and after recovery and alkalization.

4.3 Figure 5 additional data

Similarly in this test, the voltage is measured between the LFP and the 1M Ag/AgCl that was placed in the lithium reservoir during operation. The sense channel measured the voltage between LFP and Bi electrodes. Based on the K_{sp} data (Table S4) and the composition of the simulated seawater used (Table S2), $MgCO_3$ and $CaCO_3$ can thermodynamically precipitate as their ionic product is greater than Ksp value. As for the hydroxides, it is thermodynamically unfavorable unless the solution pH reaches 9.26 for $Mg(OH)_2$ and 12.4 for $Ca(OH)_2$. Given the volume of pristine seawater used during bismuth recovery, the bulk pH does not reach those values, however high local pH zones can occur.

Table S4: Solubility product constants of magnesium and calcium salts [4]

Solubility product constant (Ksp) at 25°C	$Mg(OH)_2$	$MgCO_3$	$Ca(OH)_2$	$CaCO_3$
	$1.8 \times 10^{-11}\ M^3$	$3.5 \times 10^{-8}\ M^2$	$5.5 \times 10^{-6}\ M^3$	$2.8 \times 10^{-9}\ M^2$

To remove precipitate build-up during recovery, the acidified bismuth extraction reservoir formed during the acidification step is used after alkalization to wash the bismuth side (Fig. S14). The effect of acid washing on the following bismuth acidification cycle is shown in Fig. S13 during flow cell operation for 50 ml 2.1 Mm DIC with 0.5 M NaCl with seawater impurities. During acid washing, the acidified solution is circulated at 35 mL/min through the bismuth chamber, and the pH probe is placed in the reservoir to terminate the wash once the pH stabilizes, indicating that nearly all precipitates have been neutralized and washed away.

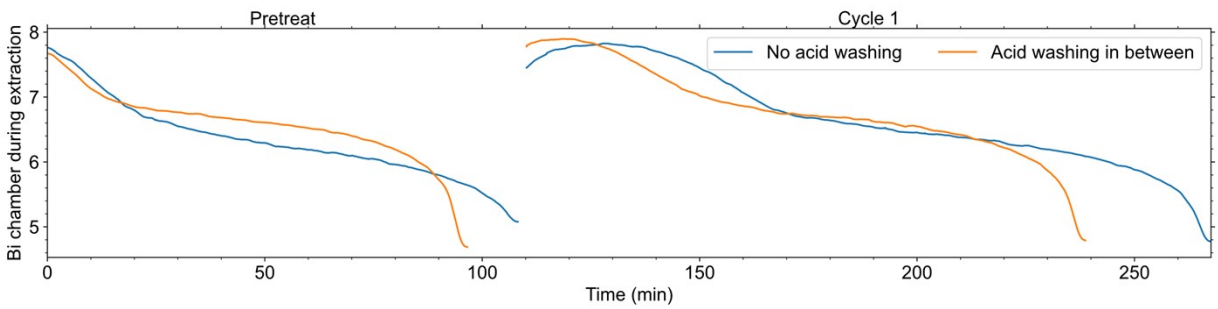

Fig. S13: Effect of acid washing on the subsequent bismuth acidification cycle in a flow cell

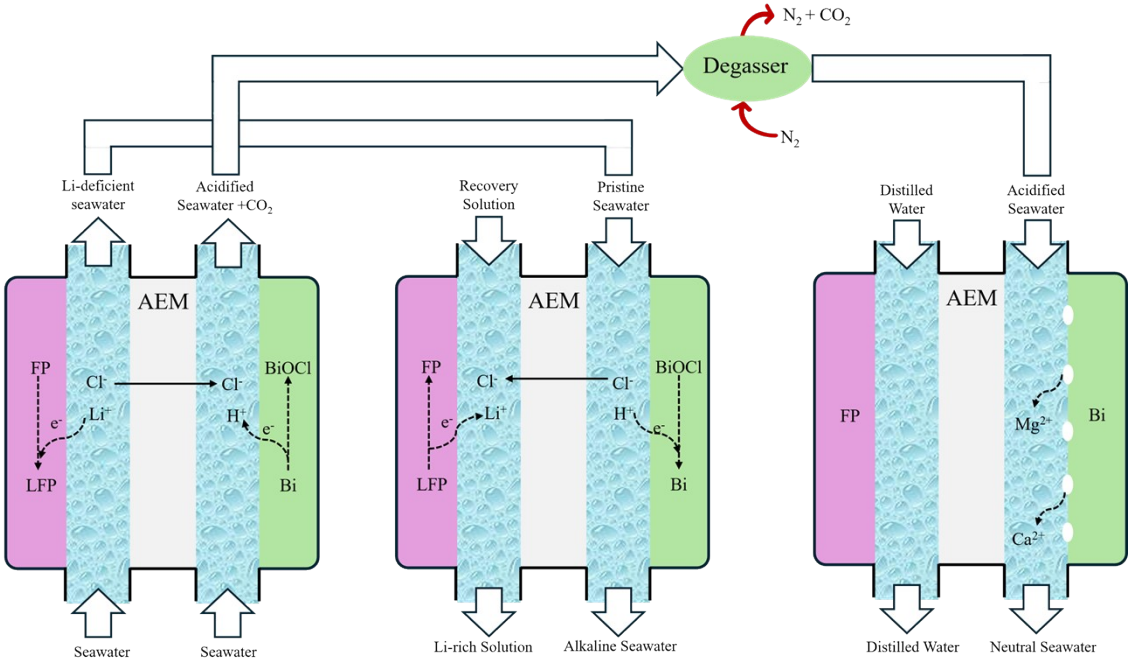

Fig. S14: Electrolyte flow in the presence of impurities in simulated seawater

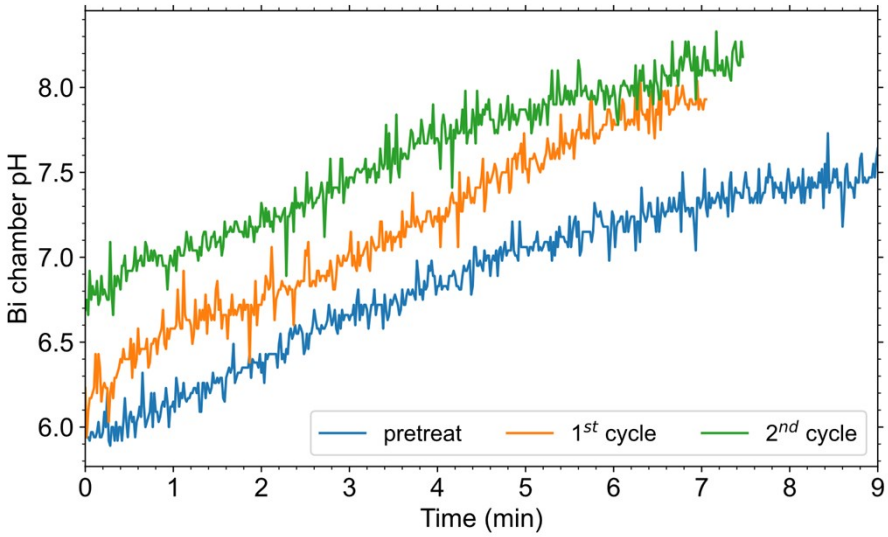

Fig. S15: Bismuth chamber raw data pH profile during acid-washing after the previous cycle alkalization step

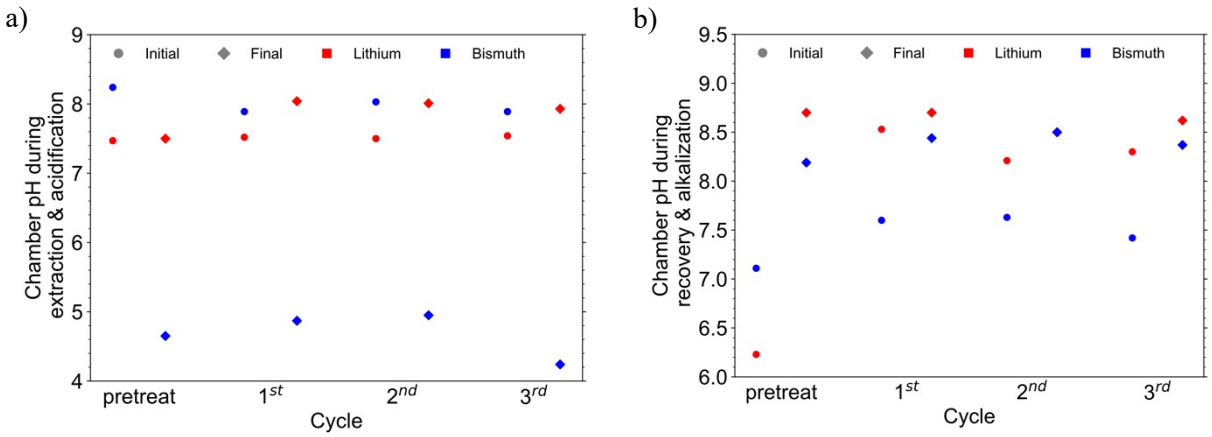

Fig. S16: Lithium and bismuth chamber pH in each cycle before and after a) extraction and acidification b) recovery and alkalization.

4.4 Figure 6a additional data

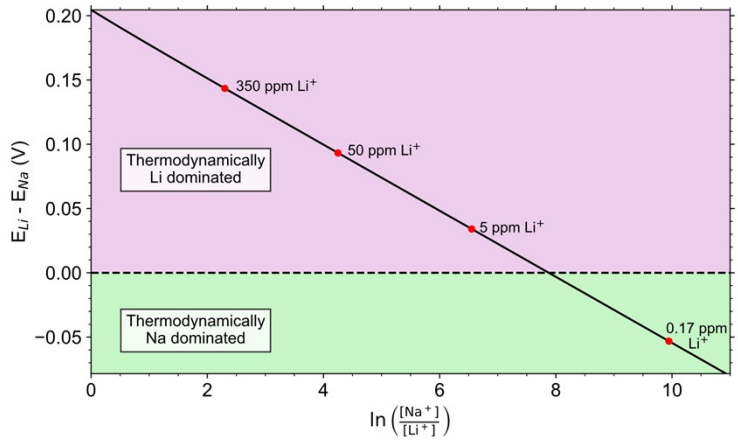

Fig. S17: Thermodynamic plot of the difference in lithium and sodium intercalation potential at 0.5M NaCl and varying lithium concentration

A thermodynamic plot comparing the co-intercalation potential of lithium and sodium at varying lithium concentration is created to understand the thermodynamic limitations of iron phosphate for lithium extraction (Fig. S17). At 350 and 50 ppm Li^+ , lithium is favored to intercalate into the iron phosphate, hence only the pretreatment method mentioned previously is sufficient to maintain a high selectivity. At 5ppm Li^+ which is closer to the borderline, and 0.17 ppm Li^+ where it is no longer thermodynamically favorable to intercalate lithium, modifications were made to the electrode and operating procedures. For the electrode, ≈3 nm of titanium oxide is coated onto the electrode surface using the atomic layer deposition (ALD) method. TiO_2 is a non-conductive hydrophilic coating that lowers the energy barrier by relying on the presence of oxygen vacancies that improves lithium-ion diffusivity [5,6]. The coating procedure was done using the GEMStar XT, plasma-enhanced ALD. The precursor chosen is TDMAT, tetrakis(dimethylamido)titanium (IV), which is heated up to 75°C, while the chamber where the electrodes are is at 200°C and −1 atmg. The deposition occurred in 80 cycles, where in each cycle the precursor was injected for 200 ms, 5 s exposure time for chemical bond to form, 15 s to purge excess TDMAT, and 20 s exposure to the 40W O_2 plasma to break down TDMAT to TiO_2 layer and lastly 5s to purge the by-product gases from the chamber.

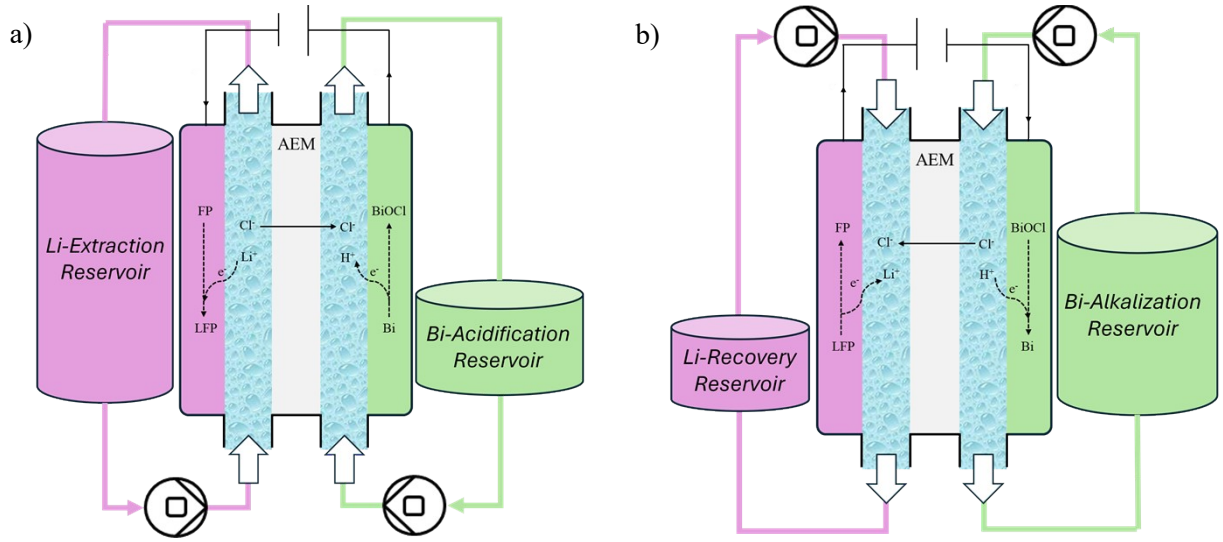

Fig. S18: Asymmetrical electrolyte flow configuration during a) extraction and acidification b) recovery and alkalization

As for the system operation, the pulse-reverse pulse method is used where a constant current is applied for 10 s, followed by 10 s at open circuit, then 2 s of reverse constant current, and 2 s at open circuit. The pulse-reverse pulse method relies on the difference in the diffusivity coefficient, as well as the ionic radius of the cations in the solution [7]. Li^+ has a lower diffusivity coefficient compared to Na^+ and Mg^{2+}, hence it has a larger concentration gradient near the electrode interface boundary layer. The 10 s pulse and 10 s rest ensure that the lithium concentration gradient does not get worse and is given time to decrease. The reverse pulse then drives cations away from the surface; ions with higher diffusivity retreat more quickly, resulting in a thicker boundary layer for Na^+ and Mg^{2+} relative to Li^+. This differential response enhances the selectivity of the subsequent pulse step.

The asymmetrical electrolyte-flow configuration is shown in Fig. S18. Because a larger lithium extraction reservoir was used, there was a higher risk of losing the ionic conduction pathway between the reservoir where the reference electrode is located and the flow cell. To address this, the potentiostat connections were modified. The measure channel was used to connect the LFP and Bi electrodes, and the sense channel measured the potential between the LFP and the 1 M Ag/AgCl reference electrode. For this test, acid washing was included after the 2nd pretreatment where impurities were introduced (Fig. S20).

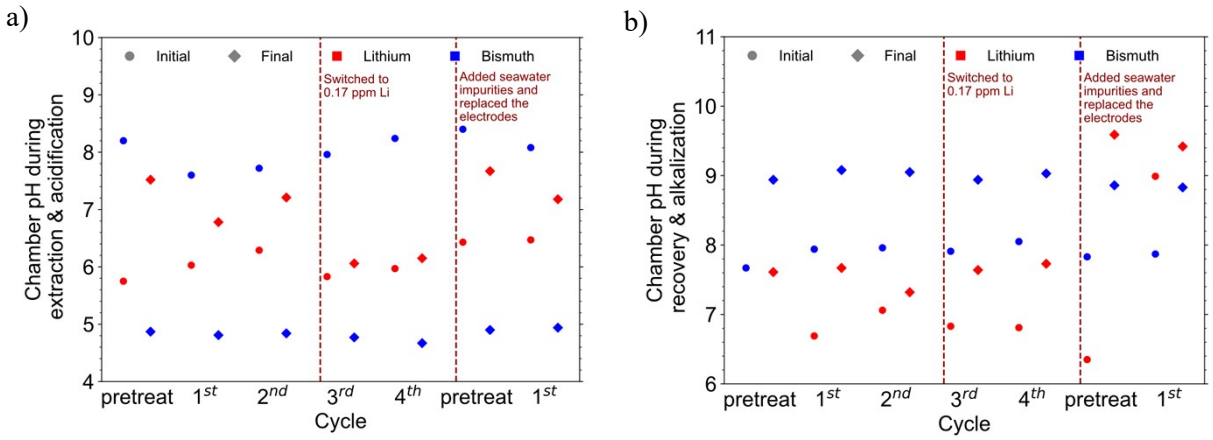

Fig. S19: Lithium and bismuth chamber pH in each cycle before and after a) extraction and acidification b) recovery and alkalization.

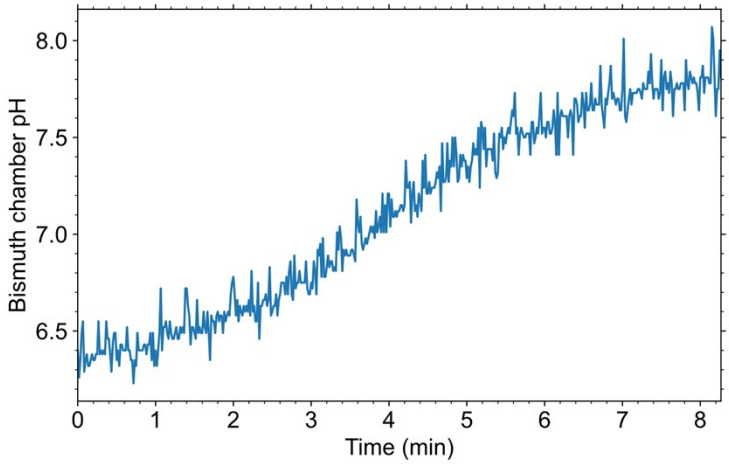

Fig. S20: Bismuth chamber raw pH profile during the acid-washing after the 2nd pretreat cycle

To obtain the Energy-Dispersive X-ray Spectroscopy (EDX) data, as well as the secondary electron (SE) images, the FEI Quanta 650 SEM is used on the electrodes after operation in the simulated seawater with impurities. EDX data were collected using a 20 kV electron beam, which provides sufficient excitation energy to generate the characteristic X-rays of all elements present. As for imaging, secondary electron (SE) was chosen to be detected to visualize the topography of the electrode after the operation (Fig. S21). Images show the presence of micrometers clusters which would reduce the active surface area and increase the overpotentials during cell operation.

a)

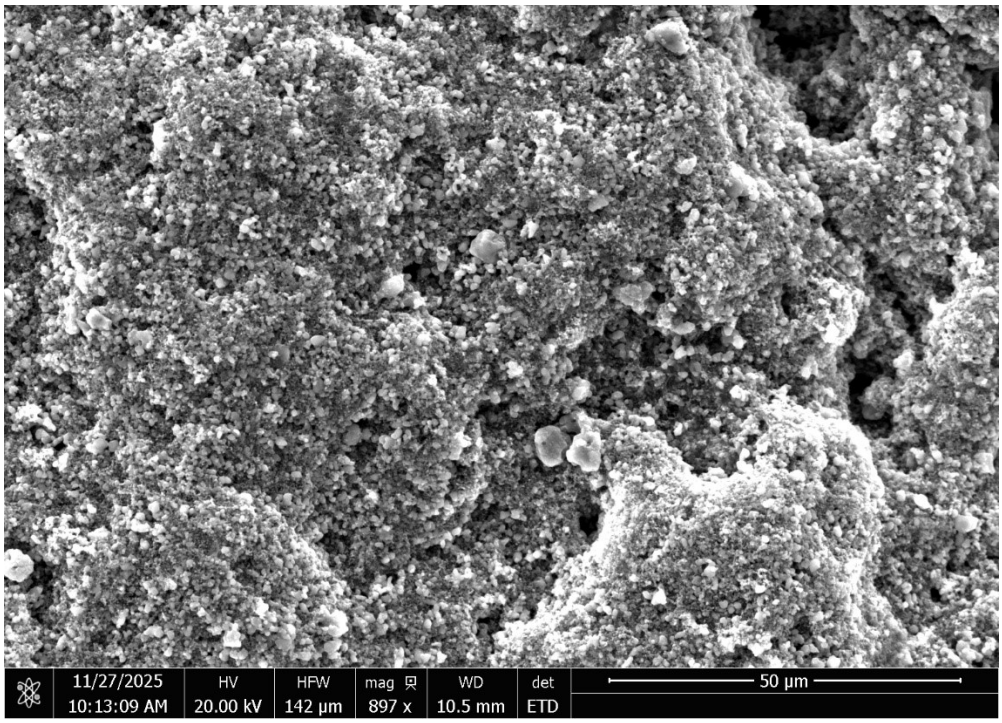

b)

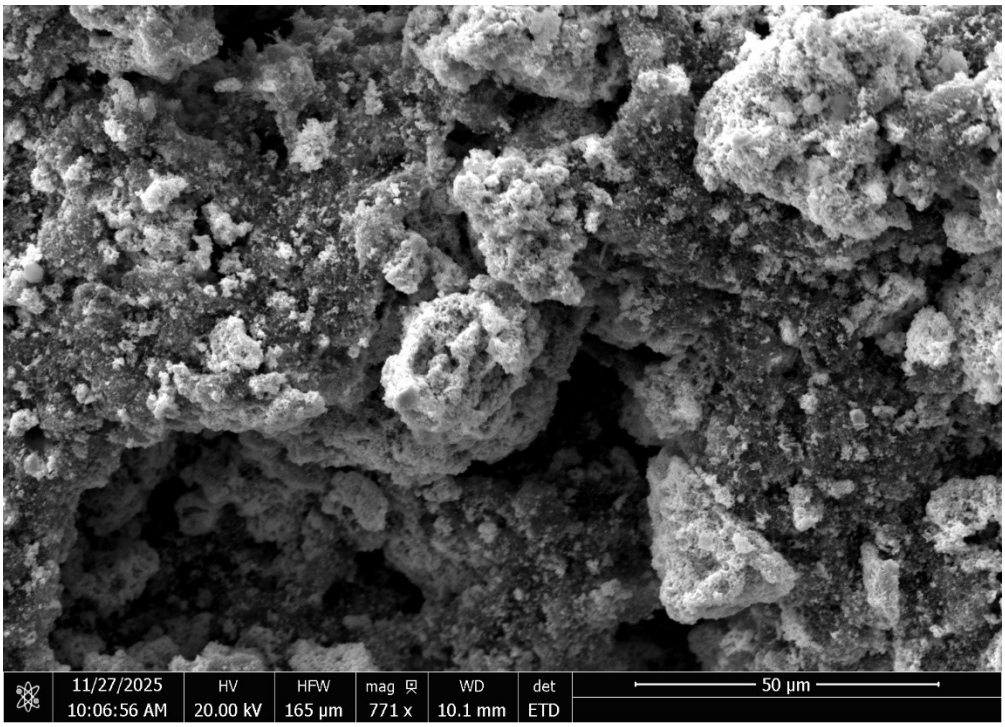

Fig. S21: SE images of a) LFP b) Bi electrode after operation in a simulated seawater with impurities

4.5 Figure 6c additional data

For the last test where simulated seawater is used without impurities and maintaining Li^+ at 0.17ppm, voltage was measured between the LFP and Bi electrodes, while the sense channel measures the voltage between the LFP and 1M Ag/AgCl electrode.

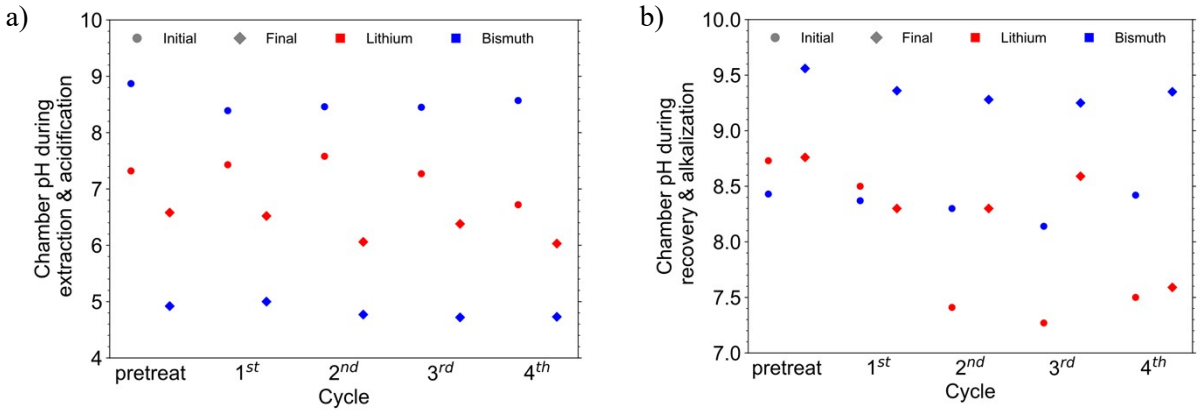

Fig. S22: Lithium and bismuth chamber pH in each cycle before and after a) extraction and acidification b) recovery and alkalization.

4.6 Voltage profiles comparison in the lithium and bismuth chamber

Comparing the lithium-chamber voltage profiles during extraction shows that the pulse–reverse-pulse method prevents the half-cell voltage from becoming progressively more negative over time. This indicates controlled lithium intercalation and ensures that extraction remains a spontaneous step as long as the two half-cell voltages do not overlap. As expected, impurities negatively affect lithium intercalation. Their influence becomes especially evident during recovery.

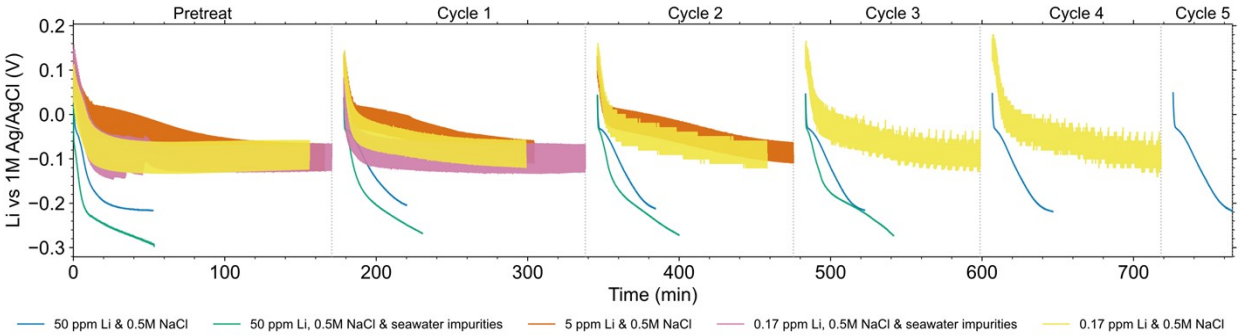

Fig. S23: Lithium chamber voltages profiles during extraction

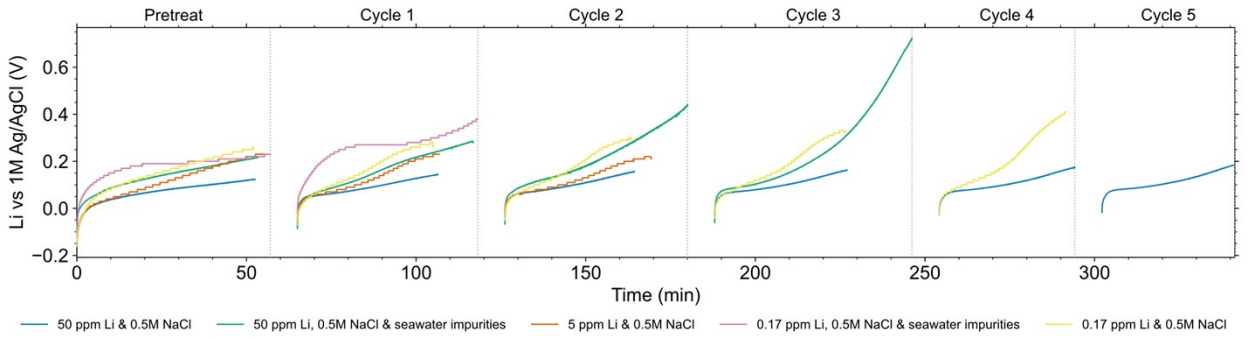

Fig. S24: Lithium chamber voltage profiles during recovery.

For the bismuth chamber, the half-cell voltage during acidification shows no noticeable change in the presence of impurities with acid-washing being implemented. During alkalization , however, impurities promote precipitate build-up, which increases the cell overpotential and the energy required. This effect is reduced by the acid-washing step, which controls the precipitation buildup over cycles. When comparing the influence of the pulse–reverse-pulse method, the bismuth half-cell voltage during alkalization becomes more positive under pulsed operation, which would lower the cell voltage and hence the energetic cost. We propose that this behavior arises from the differences in the BiOCl layer structure during formation, a material with low electrical conductivity, on the bismuth electrode surface. Under pulsation operation, instead of developing into a dense, blocking film, the BiOCl forms as dispersed clusters across the surface. This distribution creates a more porous microstructure, providing improved ion-transport pathways and enabling ions to reach active sites deeper within the electrode.

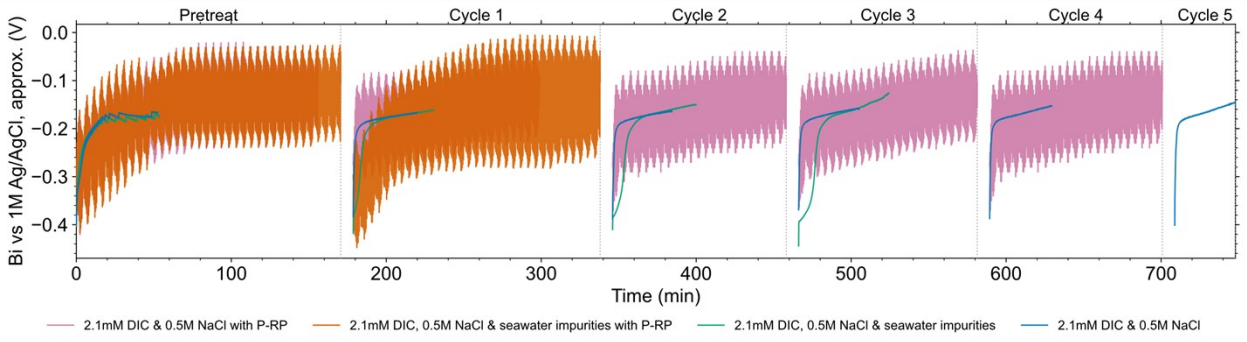

Fig. S25: Bismuth chamber voltage profiles during acidification.

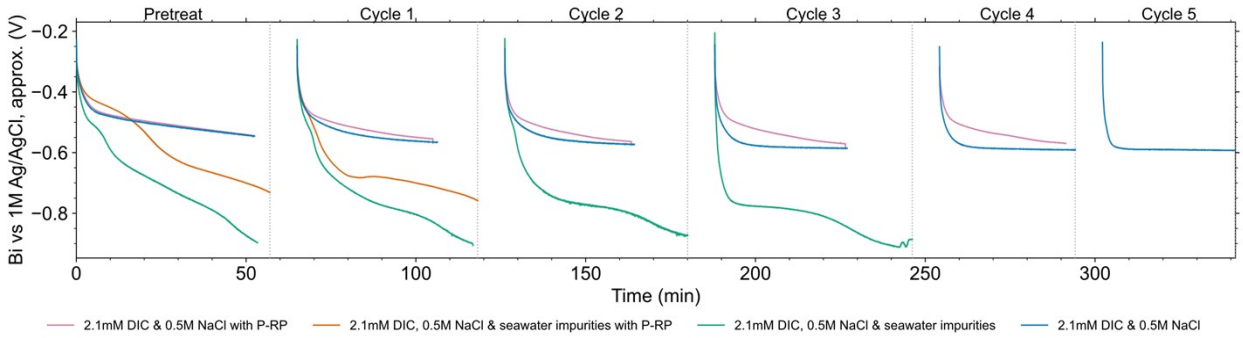

Fig. S26: Bismuth chamber voltage profiles during alkalization.

References

[1] F.J. Millero, The marine inorganic carbon cycle, Chem. Rev. 107 (2007) 308–341. https://doi.org/https://doi.org/10.1021/cr0503557.

[2] G. Yan, G. Kim, R. Yuan, E. Hoenig, F. Shi, W. Chen, Y. Han, Q. Chen, J.M. Zuo, W. Chen, C. Liu, The role of solid solutions in iron phosphate-based electrodes for selective electrochemical lithium extraction, Nature Communications 2022 13:1 13 (2022) 4579-. https://doi.org/10.1038/s41467-022-32369-y.

[3] M.E.Q. Pilson, An Introduction to the Chemistry of the Sea , Cambridge University Press, 2012.

[4] Ksp Table, (n.d.). https://www.chm.uri.edu/weuler/chm112/refmater/KspTable.html (accessed December 9, 2025).

[5] K. Liang, X. Chen, Z. Guo, T. Hou, X. Zhang, Y. Li, Lithium intercalation and diffusion in TiO2 nanotubes: a first-principles investigation, Physical Chemistry Chemical Physics 18 (2016) 24370–24376. https://doi.org/10.1039/C6CP03830A.

[6] Y. Xu, J. Mao, Enhanced electrochemical performance of LiFePO4 cathode with carbon-TiO2 hybrid coating, Journal of Materials Science 2016 51:22 51 (2016) 10026–10034. https://doi.org/10.1007/S10853-016-0229-5.

[7] C. Liu, Y. Li, D. Lin, P.C. Hsu, B. Liu, G. Yan, T. Wu, Y. Cui, S. Chu, Lithium Extraction from Seawater through Pulsed Electrochemical Intercalation, Joule 4 (2020) 1459–1469. https://doi.org/10.1016/j.joule.2020.05.017.